Research Article

An Analytical Comparison of Transfer Learning Techniques for Brain Tumor Detection and Classification

Mohammed Amin Almaiah[1, *], ⓘⒹ, Fuad Ali El-Qirem[2,] ⓘⒹ

[1] *King Abdullah the II IT School, The University of Jordan, Amman 11942, Jordan.*

[2] *Faculty of Architecture and Design, Al-Zaytoonah University of Jordan, Amman 11733, Jordan.*

ARTICLEINFO

ABSTRACT

Because brain tumors are complex, they must be diagnosed accurately and early. Brain tumor diagnosis requires expert radiologists and large datasets of annotated images, which is resource-intensive and time-consuming. This study investigates the use of transfer learning techniques to detect and classify brain tumors using MRI images. Using transfer learning, pre-trained models can be tuned to perform specific medical tasks while reducing the impact of large datasets. AlexNet, GoogleNet, ResNet-50, and VGG-16 were compared for classifying gliomas, meningioma's, and pituitary tumors based on transfer learning models. Based on the findings, the proposed hybrid GN-AlexNet model showed superior accuracy, sensitivity, specificity, and F1 score when compared with all other models, demonstrating its potential for improving brain tumor detection efficiency. The findings of this research pave the way for the adoption of transfer learning in clinical settings, providing medical professionals with more efficient and accessible solutions.

1. INTRODUCTION

A brain tumor's complexity and its nature make accurate diagnosis and classification difficult. The development of artificial intelligence and machine learning (ML) is making transfer learning increasingly important in the field of medical imaging[1]. It is possible to fine-tune large datasets without extensive labelling to meet specific tasks, resulting in high levels of accuracy and cost savings. In the study, researchers investigated whether different transfer learning approaches could be more effective at detecting and categorizing brain tumors. An analysis of transfer learning methods for detecting and classifying brain tumors. This study aims to gain a better understanding of how to leverage transfer learning in the field of neuro-oncology by evaluating different pre-trained models and their adaptability to medical imaging tasks. As a result of these findings, improved diagnostic precision and better treatment planning could result in potentially saving lives and reducing healthcare costs[2].

The term tumor also refers to a neoplasm formed when abnormal cells grow uncontrollably [3]. Brain tumors or cancer are abnormal masses of tissues in the brain or spinal canal in which small numbers of cells grow uncontrollably without being controlled by normal processes [4]. The skull encloses our brain, which is very rigid. Such a small space allows tumors to grow vigorously, which interferes with the brain's natural functions. Inorganic chemicals or genetic disorders can be major causes of deadly cancerous cells in the brain. In addition to benign tumors, there are also malignant tumors (cancers) that develop in the brain. The pressure inside people's skulls increases when benign or carcinoma tumours grow, causing several complications. There is a serious risk of traumatic brain injury and even death as a result of this. Human survival rates can be improved greatly by detecting brain tumors at an early stage. Several techniques have been proposed to predict brain tumors. Brain cancers can be classified as gliomas, meningiomas, or pituitary tumors [5]. E-healthcare has become increasingly dependent on medical imaging technology in today's environment[6]. Medical experts struggle to identify deadly brain tumor cells due to many obstacles. As the tenth most common disease, brain tumors must be diagnosed early as they pose a major threat to health. It is possible to develop a cancerous tumor of the brain in a number of different locations and at varying sizes and dimensions.

*Corresponding author. Email: malmaiah@kfu.edu.sa

For medical image analysis, various techniques are used to obtain images of the soft tissue of the human body. An MRI image is one of the images that medical experts use[7]. Using this technique, the patient's condition can be determined accurately based on the image data analysis of human brain tumors [8]. Since it normalizes tissue contrast and enhances image quality, it has a wide range of applications. MRI images can reveal brain abnormalities by providing genetic, physiological, chemistry, and biological information [9]. Depending on where they come from and how they behave, tumors can be classified into different types. A primary brain tumor originates in the central hemisphere of a vertebrate, while a secondary brain tumor originates in other organs in humans.

A glioma usually arises from a brain cell inside (gluey). (This cell is referred to as the glial cell and plays a significant role in brain cell function. World Health Organization (WHO) guidelines define grade II-III gliomas as non-glioblastic and grade IV gliomas as glioblastic [10]. Normally, tumor-producing glial cells come in three forms [11].

Since the brain and spinal cord are two of the most important control centers in the human body, any damage to them is extremely concerning. Tumors can develop anywhere on the body, and they come in many different types [12]. Today's most advanced treatments include surgery, chemotherapy, radiation, and combinations of these treatments. There is a high likelihood that patients will not survive more than 14 months, even under the most intensive medical supervision. Using these techniques, medical professionals are able to view the body in detail, giving them an in-depth understanding of symptoms and their locations. The early detection and classification of BT can enable medical professionals to plan appropriate treatment using imaging modalities, such as MRIs [13].

Additionally, BT primarily occurs in the pituitary, glioma, and meningioma glands. Tumors of the pituitary gland are usually harmless and develop in the basal layer of the brain, where they produce many important hormones [14]. In gliomas, uncontrolled growth of glial cells leads to malignancy. The central nervous system is typically supported by these cells, which are found in nerves. Brain gliomas, as well as spinal cord gliomas, can develop [15]. Brain and spinal cord membranes can be affected by cancers called meningiomas [16].

2. RELATED WORK

The term brain tumour refers to any growth of cells in or near the brain. It is possible for brain tumours to develop in the brain tissue. A brain tumor can affect the tissues in the brain as well. Several nearby structures are related to neural pathways, pituitary glands, and pineal glands [15]. Primary brain cancer is a tumour that originates in the brain. It is possible for cancer to spread to the brain from other parts of the body at times. A primary brain tumor and a metastatic brain tumor are two different types. A brain tumour may either be malignant (cancerous) or benign (non-cancerous). Surgery cannot remove malignant brain tumours, a form of cancer that is among the deadliest.

Early detection of brain tumours is essential for effective treatment [17]. There is also a difference between a primary brain tumor, which arises from brain nerves, and a metastatic tumour, which has transferred from another part of the body to the brain. In adults, about 80% of malignant brain tumors are lymphomas or gliomas of the central nervous system.

In this section, the authors outline the noteworthy research that has been conducted in the related field. Among the methods presented are largely state-of-the-art CNNs. They used a variety of CNN architectures for categorization [17], including VGGNets, GoogleNets, and ResNets, each repeated several times. According to [18], ResNet-50 performed well in the implementation, achieving 96.65% accuracy. Next, GoogleNet achieved 93.45% accuracy and VGGNets 89.33% accuracy. Additionally,[18] reported 75% and 85% accuracy levels for support vector machines and linear discriminant analyses, respectively, using leave-one-out cross-validation. Pediatric brain tumors are differentiated by a set of vital metabolites, according to a study. VGG-16, ResNet-50, and EfficientNet-B0 are among the models used [19]. It performed 99.8% better than other models when compared to EfficientNet-B0.

According to the authors of [20], this research should be carried out in five steps. In the first step, the edge of the source image is determined by linear contrast stretching. Deep neural networks are used to segment brain tumours at stage 2 using a 17-layer architecture. Step 3 involves the extraction of features using a modified MobileNetV2 architecture. System training is then based on transfer learning. Step 4 includes analyzing pituitary, meningioma, and glioma images to classify brain tumors using M-SVM. As part of step 5, entropy-based controlled techniques are combined with M-SVM (multiclass support vector machines) to select the best features. This 5-step process was found to be more accurate, both visually and numerically, than other methods, achieving 97.47% accuracy and 98.92% accuracy.

An adapted Google-Net model was used by the authors of [21], Based on Google-Net models that were fine-tuned, they achieved 93.1% accuracy. The authors used an SVM with Google-Net to achieve an accuracy of 98.1%. Inception v3, MobileNetV2, and VGG19 were CNN-based pretrained models used to classify brain X-ray images. Using ImageNet, tiny data was examined. A 93% F1 score for brain tumours and a 91% score for healthy individuals was achieved for MobileNetv2.

Additionally, the authors used a U-Net model to analyze two standard datasets, namely the 2017 and 2018 Brain Tumor Segmentation Challenges [22]. Segmentation achieved an accuracy rate of 93.40%, while classification achieved a rate of 92.20%. According to the authors, images were classified into tumour cores (TC), enhancement cores (EC), and whole

tumors (WT). Based on the comparative evaluation, it was determined that U-Net was effective. Similar to [23], the authors worked on tumour identification using hyperparameters. A better set of parameters was chosen based on the results. CNN-based U-Net models were also advocated in that study because they yielded 92% accuracy.

According to the authors, they used transfer learning to compare VGG-16, ResNet-50, and Inception v3 [11]. A 96% accuracy rate was observed for Inception v3, an 89% accuracy rate for ResNet-50, and a 75% accuracy rate for VGG-16. Based on the results, VGG-16 performed better than both other models. The authors also used a CNN-based approach [24]. The authors also used a CNN-based approach. Additionally, 25 new MRI images were tested and found to be 96% accurate. The authors in [25] investigated whether VGG-16 could be used to classify brain tumors, achieving an accuracy of 91%, which increased to 94% once hyperparameters were tuned effectively[26].

3.   METHODOLOGY

This paper describes how the GN-AlexNet deep learning model is used to classify images from the CE-MRI data set into three types of BT tumors. A CAD system for BT classification has been developed and tested. We have tested and developed the main modules of the proposed BT classification CAD system.

3.1. Brain Tumor CE-MRI Dataset

An MRI dataset that was publicly available was used by the authors for their research [27]. A total of 262 patients underwent brain MRIs at the TJU Hospital in China. The collection contains 3062 MRI images, including 1426 gliomas, 760 meningiomas, and 940 pituitary tumors. The image includes 512 x 512 layers and a size of 0.49 x 0.49 mm^2. An MRI image was used for training in this study (2146) and for testing in this study (918).

3.2. Augmenting and pre-processing data

A total of 3075 BT images are included in this dataset. The images were converted to grayscale. As well as the label of the image, these pre-processed data are one of the inputs to the neural network. Gliomas are depicted in Label 1, pituitary glands are depicted in Label 2, and meningiomas are depicted in Label 3. An effective training dataset for GN-AlexNet requires a total of 3075 MRI images. This problem can be solved through data augmentation. In this method, data is rotated and scaled, and noise is added to the already existing data to make it larger. Increasing or decreasing the brightness range of an image, rotating it horizontally or vertically, and zooming in on it will magnify the data. Through the use of all these methods, MRI images have been enhanced. Data size was increased by 16 times using augmentation methods, reducing overfitting [28].

3.3. Proposed Model

For identifying and segmenting three kinds of brain tumors (pituitary, meningioma, and glioma), this study will develop a hybrid transfer learning model that includes both AlexNet and GoogleNet. After discussing AlexNet and GoogleNet, we move on to the details of the hybrid GN-AlexNet deep learning model.

3.3.1. AlexNet

In the development of the AlexNet model, [29]. On 30 September 2012, ImageNet hosted the Large-Scale Visual Recognition Competition within AlexNet. Top-5 error rates decreased by 10.8 points (from 15.3% to 15.3%) between the network and the runner-up. Through the use of graphics processing units (GPUs) in training, the depth of the model could be adjusted in a more efficient manner.

Through the use of graphics processing units (GPUs) in training, the depth of the model could be adjusted in a more efficient manner. In contrast to only capturing low-level characteristics in the first convolutional layer, the subsequent two layers extracted high-level features. Maximizing the pooling at the end of the network increased accuracy as per Figure 1.
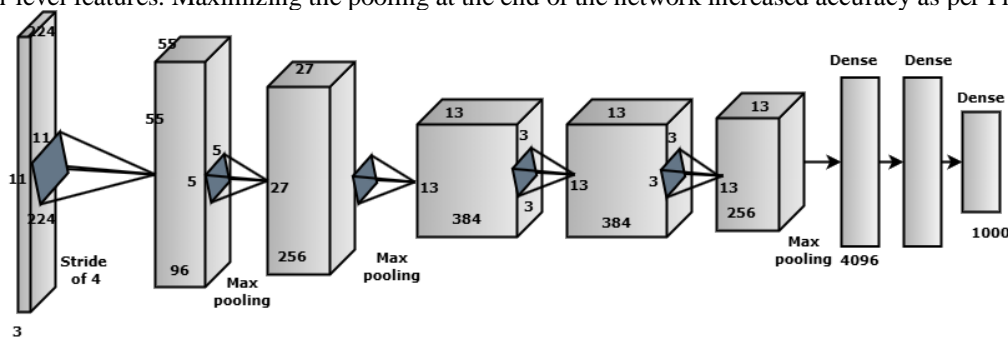

Fig. 1. AlexNet model block diagrams.

3.3.2. GoogleNeT

GN-AlexNet is a hybrid deep model combining GoogleNet with its fundamental layers. In addition to AlexNet, the model also includes. In the beginning, convolution networks can be challenging to train, and it can sometimes take several hours to complete the process. Hence, it may be more beneficial to train the proposed model with a classifier than to construct one from scratch. Ideally, this would be the best approach. ILSVRC (2014) ImageNet competition, GoogleNet's [30] Successful participation in the 2014 ImageNet competition organized by ILSVRC. Only 22 of GoogleNet's 144 layers can be learned. A total of nine modules are inception layers, two convolution layers, four maximum pooling layers, one average pooling layer, and two normalization layers. As well as the six CLS that were standard in the inception modules, each included one MX layer. In GoogleNet, new input layers have been added with dimensions $224 \times 224 \times 1$. The GooLeNet algorithm utilized activated ReLUs as part of its pre-training. A zero will be substituted for any negative value during the ReLU activation procedure. A Leaky ReLU improves performance by replacing negative values with positive ones. While developing Deep Transfer learning model, GoogleNet classifier was lost. After removing them, ten more layers were added. The leaky ReLU activation function has also been applied to the ReLU activation function in the feature map layer for improved expressiveness and to solve the dying ReLU issue.

In GoogleNet, three NIN (Network In Network) methods have been implemented: the 11 Convolution method, the global average pooling method, and the inception modules method. As shown in Figure 2a, the inception module consists of three convolutional layers including a 33-pixel pooling layer and 11-pixel convolutional layers. As the data from a lower layer is processed in parallel, the results are then sent up to the next layer in order to generate feature maps. Networking is made easier with this method. As a result of applying 11 convolutions to the inception module's internal layers, processing requirements were significantly reduced.
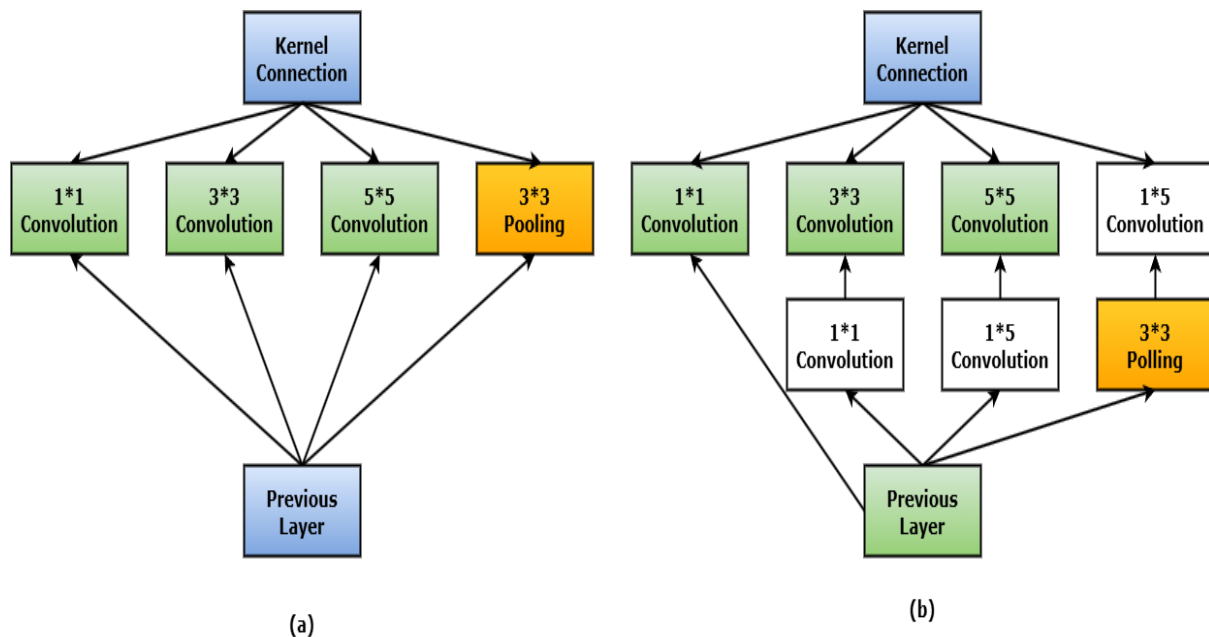

Fig. 2. GoogleNet network architecture. (a) Module without convolution. (b) Convolution Layer at inception

A convolution neural network could be modified without changing its fundamental structure. As a result of these modifications, 154 layers have been added to the previous 144. An 8 x 8 filter (patch) size reduced the image size immediately after applying the first convolution layer. Two-layer convolution network based on 1x1 convolution blocks. Reducing dimensions was the goal, so it was achieved. The GoogleNet inception module extracts features to the smallest degree with convolution kernels such as 1 by 1, 3 by 3, and 5 by 5 [31].

3.3.3. The Hybrid GN-AlexNet Model

Our model is also more expressive and the dying ReLU issue has been resolved by modifying the activation function for ReLUs in the feature map layer. With this approach, it is possible to extract more rich, more discriminative, and deeper features than state-of-the-art pretrained deep learning models. Based on a comparison of the results in Figure 3, it can be seen that classification performance has improved.
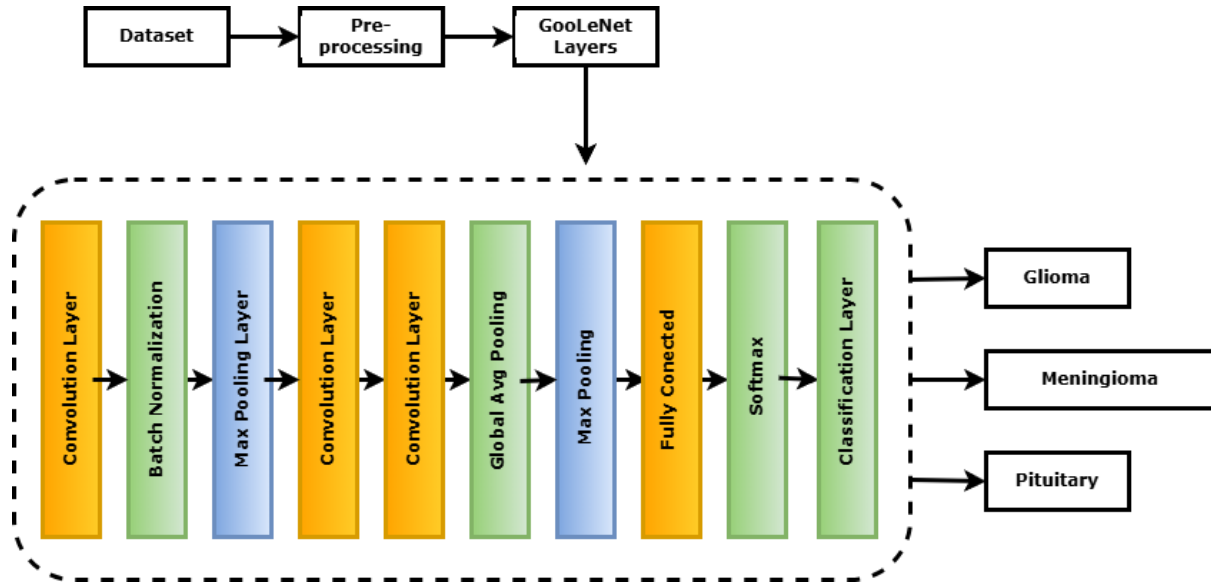
Fig. 3. The proposed GN-AlexNet model.

It consists of five layers, which include input, convolution, activation, normalization, Maxpooling, fully connected, softmax, and classification. Images are processed by the input layer after they have been received. Image inputs of dimensions 224 x 224 x 11 are used in GN-AlexNet learning models. This three-digit number indicates how wide, how high, and how many channels an image has in grayscale format. Input layers were applied before further processing. Image matrices and image filters are required as inputs to convolution layers. Input images were multiplied by the filter to produce feature maps. Here is a mathematical expression for the convolution layer: Equation (1).

$$Z_b^a = \sum_{i \in dc} K_{aj}^k * y_l^{c-1} + a_d^c \tag{1}$$

Feature maps represent both layers represented by Z_b^a and c-1 of layer D, whereas layers K and a_d^c show bias
In the activation layer, the neural network has a nonlinear activation function. Increasing the training speed is achieved through the use of rectifier linear units (ReLUs). ReLU activation is described by equation (2).

$$R(x) = \begin{cases} x & if\ x > 0 \\ 0 & if\ x \le 0 \end{cases} \tag{2}$$

As a result of the proposed convolution layers, the output parameters need to be normalized using a batch normalization layer. Normalization enables a shorter training period, leading to more efficient and effective learning. Their location dependence limits feature capture by convolutional layers. Due to this, classifications are incorrect if a feature's location changes slightly in an image. Fortunately, max-pooling can overcome this limitation by reducing the size of the representation and making it insensitive to minor changes. For the purpose of connecting the features, we used the maximum and average pools.

Fully connected layers receive features after convolutional layers have learned them. There are nodes in layers that are "fully connected" with the nodes in the layer above. Using this layer, input images can be labelled according to their class. There is a softmax layer that uses activation functions. During training, it is necessary to minimize the Loss function (H). Following the passing of all layers, an output calculation is performed. When calculating error rates based on loss functions, the desired output is subtracted from the actual output. Several iterations are necessary to minimize the loss function. Loss function was determined using categorical cross-entropy (CCE). CCE is represented mathematically by equation (3).

$$H = -H = - \sum_{m=1}^{M} y_m^l . k log\ \hat{y}_m^j \tag{3}$$

In y_m^l, sample m is predicted from M samples, and sample m is targeted from M samples.

3.3.4. VGG-16 Model.

In our experiment, we used VGG-16-trained CNNs. As a result, some convolution (Conv) layers have been frozen in order to prevent overfitting problems and avoid overfitting problems due to the small image dataset. Designed in 2014 by researchers, VGG-16 has sixteen convolution layers [15]. Brain MRI images, which have dimensions of 224 x 224 x 3, are accepted as input. In a network, the conversion layers consist of kernels with 3x3 filter sizes and 5 max-pooling layers of 2x2 dimensions [36]. A softmax output layer and extensive ReLU activation functions are included. An approximate 138

million hyperparameters are contained in the VGG-16 model. A deep neural network is constructed by stacking multiple convolutional layers in order to learn the features of invisible handcrafted products. As the model's behaviour is controlled by its hyperparameters, they are essential. In this method, the predefined loss function is minimized, and the results are improved. Several hyperparameters can be tuned, including the number of neurons, the number of epochs, softmax activation functions, learning rates, and optimizers. To tune a hyperparameter, you must first determine how many convolution layers it should have.

Thus, as ConvNet depth increases, hidden features can be learned at a subordinate cost. An overview of the VGG-16 ConvNet architecture can be seen in the figure below.

3.3.5. ResNet-50 Model.

Developed by Microsoft Research in 2015 [12], ResNet50 is a 50-layer Residual Network comprised of 26M parameters. Residual Networks use the concept of feature subtraction to refer to residuals. Instead of adding features to a layer, we learn from the subtraction of features and inputs into the layer. As compared to conventional deep CNNs, ResNet50 requires less training time. Based on the ImageNet database, a pretrained model is developed [1]. Therefore, these networks are more accurate in classifying images. In addition to skip connections, it normalizes a large number of batches at once. A gated recurrent unit or a gated unit specifies these skip connectivity. In order to create a deep neural network, an input from an nth a layer is connected directly to an $(n + x)^{th}$ layer.

As compared with VGG16 or VGG19 models, this Residual Network is less complex in terms of time complexity. We calibrated a pretrained ResNet50 model for use in our experiment.

3.3.6. Performance metric evaluation

It is proposed that a number of metrics should be measured in order to assess the effectiveness of the model, including accuracy, precision, recall, sensitivity, specificity, and F1-score. A confusion matrix shows the model's predictions based on untested examples as well as its predictions class-by-class. In subsequent subsections, each evaluation metric will be discussed in more detail following a brief description.

- **Sensitivity (Se)**

To determine whether a patient has a brain tumor, a model must be sensitive and recallable, especially for categorizing brain tumors. Additionally, we evaluate this model on the basis of accuracy, precision, recall, sensitivity, specificity, and F1-score. For the calculation of model sensitivity and recall, here is a formula:

$$Sensitivity\ (Se) = \frac{TP}{TP + FN} \tag{4}$$

- **Specificity (Sp)**

As a measure of how often predicted negative labels are actually negative, specificity is called the true negative rate (TNR). In the following equation, we present the formula for computing specificity,

$$Specificity\ (Sp) = TNR = \frac{TN}{TN + FP} \tag{5}$$

- **Accuracy (Acc)**

To determine the accuracy of the model, the number of correctly predicted labels is compared to the total number of labels. Comparing the number of correctly predicted labels to the total number of labels is one way to determine a model's accuracy. In classification tasks, precision is a key evaluation metric, and a formula is available for calculating it.

$$Accuracy\ (Acc) = \frac{TP}{TP + TN + FP + FN} \tag{6}$$

- **F1-score**

F1 scores are often referred to as F-measures due to their correlation with accuracy and recall. Measuring the model's overall performance with this metric is comprehensive. F1-score highlights the importance of balancing precision and recall. Below, you will find the formula that is used to calculate the F1 score,

$$F1 - Score = \frac{2 * Pr * Recall}{Pr + Recall} \tag{7}$$

- **Confusion matrix**

The confusion matrix, or error matrix as it is sometimes called, contains data about actual labels and predicted class assignments (ground truth). In this paper, the model's generalizability and overall performance are discussed in detail. An explanation matrix contains y-axis ground truth and x-axis predicted labels.

4. RESULTS AND DISCUSSION

Analyses of the F1 score, sensitivity, specificity, and accuracy are conducted between AlexNet and a proposed model. The graph below shows the performance results of both models. Purple bars represent the proposed model, while orange bars

represent AlexNet. Consequently, the proposed model performs better when it comes to correctly classifying positive and negative cases and dealing with imbalanced data. The performance of the proposed model is clearly improved over that of AlexNet, a widely known architecture. These findings suggest that the proposed model would provide enhanced results for these key evaluation categories, indicating its suitability. The accuracy rate of AlexNet was 95.60 percent, which is an excellent result.
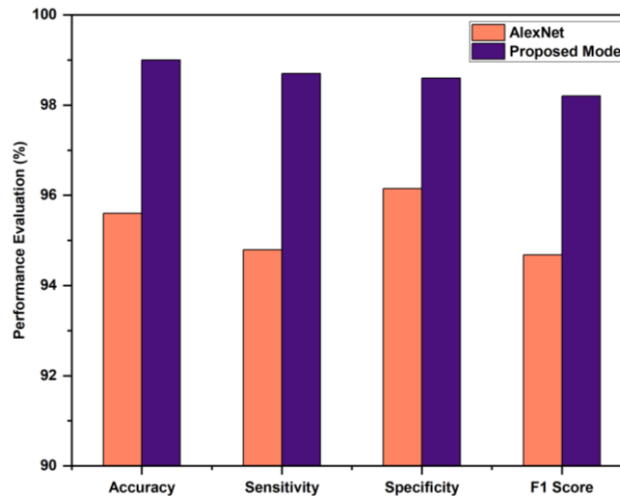

Fig. 4. Performance evaluation of the proposed model's.

All metrics show that the proposed model outperforms the VGG-16 model. A purple bar indicates the proposed model is more accurate, sensitive, specific, and has a higher F1 score than an orange bar. According to this, the proposed model is better able to identify positive and negative cases, as well as to cope with class imbalances, than the VGG-16 model. In this particular evaluation, the proposed model appears to deliver more reliable and robust results than the VGG-16 architecture. The VGG16 model achieved 97.66% accuracy.
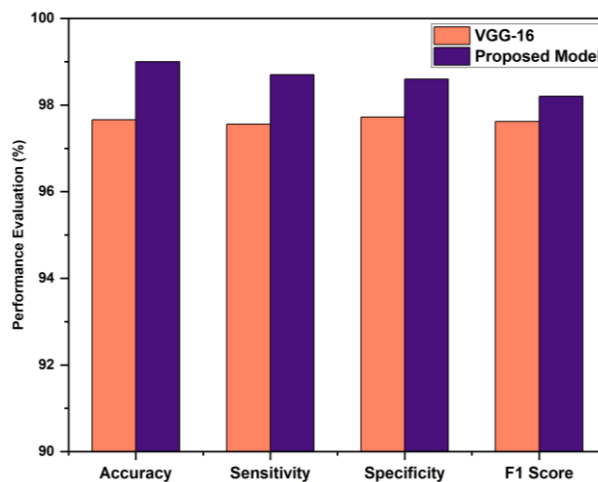

Fig. 5. Proposed model comparison of the proposed model with existing model.

All evaluated metrics show that the proposed model performs better than ResNet-50. Purple bars (proposed model) are higher than orange bars (ResNet-50), indicating that the proposed model is more accurate, sensitive, specific, and F1. Compared to ResNet-50, the proposed model correctly identifies positive and negative cases, handles class imbalances better, and provides higher overall classification accuracy. In these important evaluation categories, the proposed model proved to be more robust and reliable than ResNet-50. ResNet-50 achieves 96.90% accuracy, which is an impressive achievement for a model of this type.
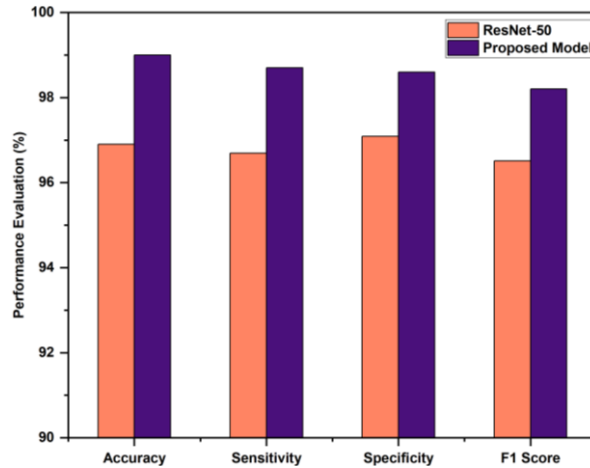
Fig. 6. Proposed model performance compared to the ResNet-50.

Based on all four evaluation categories, purple bars consistently performed better than orange bars. In terms of accuracy, sensitivity, specificity, and F1, the proposed model performs near-perfectly, while GoogleNet performs significantly worse, particularly on sensitivity and specificity. Hence, the proposed model can correctly identify positive and negative cases and handle imbalanced data. GoogleNet, on the other hand, performs much less well. Considering the large difference between these results, the proposed model is more efficient and robust than GoogleNet, making it a perfect fit for the task. GoogleNet's accuracy is 98.99%.
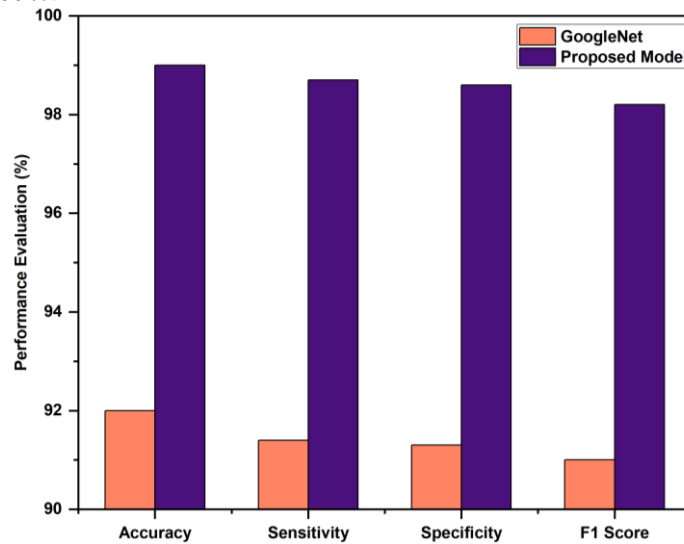

Fig. 7. Proposed model performance compared to the Google-Net.

5.   CONCLUSION

Using MRI images, this study compares various transfer learning models for detecting brain tumors. As a result, the proposed hybrid GN-AlexNet model demonstrates significantly superior accuracy, sensitivity, specificity, and F1 score to AlexNet, GoogleNet, ResNet-50, and VGG-16. Based on its superior performance, it could lead to more accurate and reliable brain tumor classifications that could improve early diagnosis and treatment planning. The use of transfer learning, especially when combined with data augmentation, has proven a valuable method to overcome challenges related to the limited amount of labelled data and the efficiency of model training. Future efforts should focus on further optimization, evaluating the model's performance on a larger and more diverse dataset, and exploring how it can be deployed in clinical settings to assist healthcare professionals in diagnosing brain tumors.

References

[1] S. P. Yadav, M. Jindal, P. Rani, V. H. C. de Albuquerque, C. dos Santos Nascimento, and M. Kumar, "An improved deep learning-based optimal object detection system from images," *Multimedia Tools and Applications*, vol. 83, no. 10, pp. 30045–30072, 2024.

[2] P. Rani, P. N. Singh, S. Verma, N. Ali, P. K. Shukla, and M. Alhassan, "An implementation of modified blowfish technique with honey bee behavior optimization for load balancing in cloud system environment," *Wireless Communications and Mobile Computing*, vol. 2022, pp. 1–14, 2022.

[3] C. L. Choudhury, C. Mahanty, R. Kumar, and B. K. Mishra, "Brain Tumor Detection and Classification Using Convolutional Neural Network and Deep Neural Network," in *2020 International Conference on Computer Science, Engineering and Applications (ICCSEA)*, Gunupur, India: IEEE, Mar. 2020, pp. 1–4. doi: 10.1109/ICCSEA49143.2020.9132874.

[4] D. Dheeraj and H. S. Prasantha, "Study of machine learning vs. deep learning algorithms for detection of tumor in human brain," *International Journal of Computer Science and Engineering*, vol. 8, no. 1, pp. 2347–2693, 2020.

[5] H. Barad and A. Patel, "Application of machine learning and deep learning methods for brain tumor identification and classification," *International Journal of Recent Technology and Engineering*, vol. 86, 2020, Accessed: Mar. 16, 2025. [Online]. Available: https://www.academia.edu/download/90912342/F8062038620.pdf

[6] P. Rani and M. H. Falaah, "Real-Time Congestion Control and Load Optimization in Cloud-MANETs Using Predictive Algorithms," *NJF Intelligent Engineering Journal*, vol. 1, no. 1, pp. 66–76, 2024.

[7] P. Rani, S. P. Yadav, P. N. Singh, and M. Almusawi, "Real-World Case Studies: Transforming Mental Healthcare With Natural Language Processing," in *Demystifying the Role of Natural Language Processing (NLP) in Mental Health*, A. Mishra, S. P. Yadav, M. Kumar, S. M. Biju, and G. C. Deka, Eds., IGI Global, 2025, pp. 303–324. doi: 10.4018/979-8-3693-4203-9.ch016.

[8] M. Talo, U. B. Baloglu, Ö. Yıldırım, and U. Rajendra Acharya, "Application of deep transfer learning for automated brain abnormality classification using MR images," *Cognitive Systems Research*, vol. 54, pp. 176–188, May 2019, doi: 10.1016/j.cogsys.2018.12.007.

[9] A. Gudigar, U. Raghavendra, T. R. San, E. J. Ciaccio, and U. R. Acharya, "Application of multiresolution analysis for automated detection of brain abnormality using MR images: A comparative study," *Future Generation Computer Systems*, vol. 90, pp. 359–367, Jan. 2019, doi: 10.1016/j.future.2018.08.008.

[10] M. Visser *et al.*, "Inter-rater agreement in glioma segmentations on longitudinal MRI," *NeuroImage: Clinical*, vol. 22, p. 101727, 2019, doi: 10.1016/j.nicl.2019.101727.

[11] H. A. Khan, W. Jue, M. Mushtaq, and M. U. Mushtaq, "Brain tumor classification in MRI image using convolutional neural network," *Mathematical Biosciences and Engineering*, 2021, Accessed: Mar. 16, 2025. [Online]. Available: https://papers.ssrn.com/sol3/Delivery.cfm?abstractid=3894961

[12] E. G. Van Meir, C. G. Hadjipanayis, A. D. Norden, H. K. Shu, P. Y. Wen, and J. J. Olson, "Exciting New Advances in Neuro-Oncology: The Avenue to a Cure for Malignant Glioma," *CA: A Cancer Journal for Clinicians*, vol. 60, no. 3, pp. 166–193, May 2010, doi: 10.3322/caac.20069.

[13] M. Saddique, J. H. Kazmi, and K. Qureshi, "A Hybrid Approach of Using Symmetry Technique for Brain Tumor Segmentation," *Computational and Mathematical Methods in Medicine*, vol. 2014, pp. 1–10, 2014, doi: 10.1155/2014/712783.

[14] J. Komninos *et al.*, "Tumors Metastatic to the Pituitary Gland: Case Report and Literature Review," *The Journal of Clinical Endocrinology & Metabolism*, vol. 89, no. 2, pp. 574–580, Feb. 2004, doi: 10.1210/jc.2003-030395.

[15] L. M. DeAngelis, "Brain Tumors," *N Engl J Med*, vol. 344, no. 2, pp. 114–123, Jan. 2001, doi: 10.1056/NEJM200101113440207.

[16] D. N. Louis *et al.*, "The 2016 World Health Organization Classification of Tumors of the Central Nervous System: a summary," *Acta Neuropathol*, vol. 131, no. 6, pp. 803–820, Jun. 2016, doi: 10.1007/s00401-016-1545-1.

[17]   A. Gumaei, M. M. Hassan, M. R. Hassan, A. Alelaiwi, and G. Fortino, "A Hybrid Feature Extraction Method With Regularized Extreme Learning Machine for Brain Tumor Classification," *IEEE Access*, vol. 7, pp. 36266–36273, 2019, doi: 10.1109/ACCESS.2019.2904145.

[18]   D. Zhao *et al.*, "Metabolite selection for machine learning in childhood brain tumour classification," *NMR in Biomedicine*, vol. 35, no. 6, p. e4673, Jun. 2022, doi: 10.1002/nbm.4673.

[19]   V. Agrawal, M. Hazratifard, H. Elmiligi, and F. Gebali, "Electrocardiogram (ECG)-Based User Authentication Using Deep Learning Algorithms," *Diagnostics*, vol. 13, no. 3, p. 439, Jan. 2023, doi: 10.3390/diagnostics13030439.

[20]   S. Maqsood, R. Damaševičius, and R. Maskeliūnas, "Multi-Modal Brain Tumor Detection Using Deep Neural Network and Multiclass SVM," *Medicina*, vol. 58, no. 8, p. 1090, Aug. 2022, doi: 10.3390/medicina58081090.

[21]   M. Rasool *et al.*, "A Hybrid Deep Learning Model for Brain Tumour Classification," *Entropy*, vol. 24, no. 6, p. 799, Jun. 2022, doi: 10.3390/e24060799.

[22]   K. R. Pedada, B. R. A., K. K. Patro, J. P. Allam, M. M. Jamjoom, and N. A. Samee, "A novel approach for brain tumour detection using deep learning based technique," *Biomedical Signal Processing and Control*, vol. 82, p. 104549, Apr. 2023, doi: 10.1016/j.bspc.2022.104549.

[23]   B. Kokila, M. S. Devadharshini, A. Anitha, and S. A. Sankar, "Brain tumor detection and classification using deep learning techniques based on MRI images," in *Journal of Physics: Conference Series*, IOP Publishing, 2021, p. 012226. Accessed: Mar. 16, 2025. [Online]. Available: https://iopscience.iop.org/article/10.1088/1742-6596/1916/1/012226/meta

[24]   B. Ahmed Mohammed, M. Shaban Al-Ani, University of Human Development, College of Science and Technology, Department of Computer Science, Sulaymaniyah, KRG, Iraq and University of Sulaimani, College of Science, Department of Computer, Sulaymaniyah, KRG, Iraq, and University of Human Development, College of Science and Technology, Department of Information Technology, Sulaymaniyah, KRG, Iraq, "An efficient approach to diagnose brain tumors through deep CNN," *Mathematical Biosciences and Engineering*, vol. 18, no. 1, pp. 851–867, 2021, doi: 10.3934/mbe.2021045.

[25]   P. Gayathri, A. Dhavileswarapu, S. Ibrahim, R. Paul, and R. Gupta, "Exploring the potential of vgg-16 architecture for accurate brain tumor detection using deep learning," *Journal of Computers, Mechanical and Management*, vol. 2, no. 2, pp. 13–22, 2023.

[26]   S. Verma *et al.*, "An automated face mask detection system using transfer learning based neural network to preventing viral infection," *Expert Systems*, vol. 41, no. 3, p. e13507, Mar. 2024, doi: 10.1111/exsy.13507.

[27]   "Resize Function. Available online:" Accessed: Mar. 15, 2025. [Online]. Available: https://www.mathworks.com/products/matlab.html

[28]   S. Jégou, M. Drozdzal, D. Vazquez, A. Romero, and Y. Bengio, "The one hundred layers tiramisu: Fully convolutional densenets for semantic segmentation," in *Proceedings of the IEEE conference on computer vision and pattern recognition workshops*, 2017, pp. 11–19. Accessed: Mar. 15, 2025. [Online]. Available: http://openaccess.thecvf.com/content_cvpr_2017_workshops/w13/html/Jegou_The_One_Hundred_CVPR_2017_paper.html

[29]   A. Krizhevsky, I. Sutskever, and G. E. Hinton, "ImageNet classification with deep convolutional neural networks," *Commun. ACM*, vol. 60, no. 6, pp. 84–90, May 2017, doi: 10.1145/3065386.

[30]   C. Szegedy *et al.*, "Going deeper with convolutions," in *Proceedings of the IEEE conference on computer vision and pattern recognition*, 2015, pp. 1–9. Accessed: Mar. 15, 2025. [Online]. Available: https://www.cv-foundation.org/openaccess/content_cvpr_2015/html/Szegedy_Going_Deeper_With_2015_CVPR_paper.html

[31]   J. Bai, H. Jiang, S. Li, and X. Ma, "NHL Pathological Image Classification Based on Hierarchical Local Information and GoogLeNet-Based Representations," *BioMed Research International*, vol. 2019, pp. 1–13, Mar. 2019, doi: 10.1155/2019/1065652.